CHEMICAL PHYSICS

Capacitance of thin films containing polymerized ionic liquids

Rajeev Kumar[1,2,3]*, Jyoti P. Mahalik[1,3], Kevin S. Silmore[4], Zaneta Wojnarowska[5], Andrew Erwin[6,7], John F. Ankner[8], Alexei P. Sokolov[6,9,10], Bobby G. Sumpter[1,2], Vera Bocharova[6]*

Electrode-polymer interfaces dictate many of the properties of thin films such as capacitance, the electric field experienced by polymers, and charge transport. However, structure and dynamics of charged polymers near electrodes remain poorly understood, especially in the high concentration limit representative of the melts. To develop an understanding of electric field–induced transformations of electrode-polymer interfaces, we have studied electrified interfaces of an imidazolium-based polymerized ionic liquid (PolyIL) using combinations of broadband dielectric spectroscopy, specular neutron reflectivity, and simulations based on the Rayleigh's dissipation function formalism. Overall, we obtained the camel-shaped dependence of the capacitance on applied voltage, which originated from the responses of an adsorbed polymer layer to applied voltages. This work provides additional insights related to the effects of molecular weight in affecting structure and properties of electrode-polymer interfaces, which are essential for designing next-generation energy storage and harvesting devices.

INTRODUCTION

The electrical double layer (EDL) (*1*–*7*) is a universal feature of electrified interfaces in all ionic materials. Spontaneous formation of the double layer is one of the primary mechanisms for storing electrical energy in devices such as supercapacitors (*8*). Understanding correlations between structure and properties of EDLs is vital for achieving control over device characteristics such as capacitance of electrochemical storage devices as well as charging and discharging rates of batteries. In the last two decades, special attention has been devoted to EDLs in highly concentrated electrolytes such as room temperature ionic liquids (ILs) (*6*, *7*, *9*–*14*) because of their relevance for a number of applications. Specifically, a number of theoretical, simulation, and experimental reports (*6*, *7*, *9*–*14*) have focused on understanding the structural changes of EDLs in an applied electric field and their connections with charge storage properties. As a result of such an extensive research, an interplay of electrostatics and crowding effects, resulting from finite size of ions, has been identified to be responsible for the anatomy of the EDLs in ILs. The EDLs in ILs have been shown to exhibit the layering of ions (*11*) and non-monotonic dependence of the screening length on the concentration of ions in solutions of ILs (*14*).

Experimentally, the short-range, surface-induced ordering of ions within ~1 nm from surfaces has been confirmed with x-ray scattering (*15*). In contrast, recent surface force apparatus measurements (*16*) of ILs demonstrated the presence of an EDL of width equal to approximately 35 ionic diameters per surface, leading to a representation of ILs as very weakly dissociated electrolyte solutions (*16*). On the basis of the structure of the EDL, different shapes of capacitance curves as a function of applied voltages have been obtained for ILs. These shapes include bell-shaped, U-shaped, and camel-shaped curves (*6*, *7*) in contrast to the capacitance-voltage curves observed in dilute electrolyte solutions, which are primarily U-shaped (*1*–*5*). Kornyshev (*6*) suggested an analytical model that takes into account contributions from steric exclusions between the ions, lattice saturation effects, and electrostatics, which explains the three shapes of capacitance-voltage curves. In addition, molecular simulations and experiments (*17*–*19*) showed that factors such as the chemistry of the electrolyte (*7*), electronic polarizabilities of the surface and electrolyte (*20*), the electrode surface topography (*21*, *22*), porosity (*23*–*25*), and temperature (*26*) can markedly influence the EDL structure and dependence of the capacitance on the applied voltage for ILs.

In contrast, little is known about the capacitance of polymer electrolytes, specifically in the polymeric analogs of ILs known as polymerized ionic liquids (PolyILs). PolyILs (*27*, *28*) are promising as solvent-free organic electrolytes for application in batteries, solar cells, electroactuators, and supercapacitors. They have tunable mechanical properties and high stability, and they are nonflammable. Because of their structural organization with one ion mobile and another attached to the polymer chain, several phenomena can be expected. When a bias voltage is applied across an IL, it is generally accepted that the cations migrate toward the negative electrode and the anions migrate toward the positively charged electrode, resulting in an EDL layer of similar structures on both electrodes. However, it is not clear what would be the structure of an EDL in PolyILs where one ion has limited mobility due to its covalent attachment to the polymer chain. However, some hints can be found from molecular dynamics (MD) simulations of ILs where cations and anions have different sizes (*7*, *21*). It has been shown that increasing the size of the ion (bead) can effectively change the shape of the capacitance curve from a bell to a camel shape and change the symmetry of the curve. In PolyILs, where all monomers are connected, the change in the shape should be potentially amplified, and different kinetics of EDL layer formation is expected on the cathode and

[1]Center for Nanophase Materials Sciences, Oak Ridge National Laboratory, Oak Ridge, TN 37831, USA. [2]Computational Sciences and Engineering Division, Oak Ridge National Laboratory, Oak Ridge, TN 37831, USA. [3]Department of Mathematics, University of Tennessee, Knoxville, TN 37996, USA. [4]Chemical Engineering, Massachusetts Institute of Technology, Cambridge, MA 02139, USA. [5]Institute of Physics,University of Silesia,SMCEBI, 75 Pulku Piechoty 1A, 41-500 Chorzow, Poland. [6]Chemical Sciences Division, Oak Ridge National Laboratory, Oak Ridge, TN 37831, USA. [7]School of Materials Science and Engineering, Georgia Tech, Atlanta, GA 30332, USA. [8]Neutron Scattering Division, Oak Ridge National Laboratory, Oak Ridge, TN 37831, USA. [9]Department of Physics and Astronomy, University of Tennessee, Knoxville, TN 37996, USA. [10]Department of Chemistry, University of Tennessee, Knoxville, TN 37996, USA.
*Corresponding author. Email: kumarr@ornl.gov (R.K.); bocharovav@ornl.gov (V.B.)

anode because of the different mobilities of the ions, which could potentially lead to improved charge storage properties.

In this work, we have investigated electrode-polymer interfaces of a positively charged PolyIL–poly(*N*-vinyl ethyl imidazolium) with bis(trifluoromethane)sulfonimide as counterions. We have used combinations of broadband dielectric spectroscopy (BDS) and modeling of electrode polarization phenomena by the Rayleighian approach (*29*–*31*) to extract capacitance of electrode-polymer interfaces. These combined studies resulted in capacitance-voltage curves for the PolyIL films. Furthermore, specular neutron reflectivity (*32*–*35*) is used to study structure of polymers adsorbed on the electrode in the absence of an electric field. The model based on the Rayleighian approach (*29*–*31*) was used to understand the effects of polymer chain length on the capacitance-voltage curves, which is important for designing systems with improved storage properties.

RESULTS AND DISCUSSION

Representative BDS spectra measured at different frequencies and applied DC voltages are shown in Fig. 1A. The experimental protocol for varying the applied voltage is shown schematically in Fig. 1B. The spectra contain three different regions related to the rattling of ions in a Coulombic cage at high frequencies, followed by a DC plateau and the electrode polarization at lower frequencies. As seen from comparisons of different spectra acquired at different DC bias (cf. Fig. 1A), the noticeable changes in the spectra are observed only in the region of electrode polarization at lower frequencies. The electrode polarization process becomes noticeable when ions accumulate on the electrodes, and part of the spectra representing the electrode polarization carries information about the capacitance-voltage relations.

Determining practically important thicknesses of adsorbed and diffuse layers along with capacitance from impedance spectroscopy is typically (*36*) done by fitting with equivalent electrical circuitry models. Although useful, the physical interpretation of extracted quantities using equivalent circuits poses some serious challenges and remains troublesome. In contrast, we have used an electrode polarization model for extracting capacitance at the steady state from the BDS spectra. The model was developed using the Rayleighian approach in our previous work (*31*). In the model, each electrode was assumed to have a layer of low-dielectric material in contact with polymeric film of uniform static dielectric constant (cf. Fig. 1C). The model was used to interpret kinetics of charging in similar PolyILs using BDS measurements (*31*), and excellent agreements with the pulse field gradient–nuclear magnetic resonance (PFG-NMR)–based measurements (for diffusion constants of counterions) were obtained. The measured BDS spectra of PolyILs were fitted by eq. A-5 in the Supplementary Materials. An example of the fitting is presented in Fig. 1D. From the fitting, the apparent thickness of the low-dielectric layer (λ_s) and the length scale of the mutual diffusion (L_m) were extracted. Physically, L_m represents a length scale below which electrostatics and crowding effects are substantial. L_m is proportional to the Debye screening length (see eq. A-10 in the Supplementary Materials). However, it can be greater than the screening length owing to the crowding effects included in the calculations. Both λ_s and L_m are plotted in Fig. 2A for the PolyIL films studied at 370 K.

Figure 2A shows that thickness of the low-dielectric layer (λ_s) had a nonmonotonic dependence on the applied voltage exhibiting a finite nonzero value at zero bias, followed by an initial decrease before increasing and leveling off with increase in DC voltage. Furthermore, in the experiments with different polarities of applied DC bias, the positive and negative wings had almost the same values at the minima (corresponding to λ_s = 2.47 and 2.28 nm for 0.7 and −1.3 V, respectively), suggesting almost symmetric capacitance-voltage relations shown in Fig. 2B. In contrast, the length scale of mutual diffusion (L_m) was unchanged with the applied voltage, suggesting that we are in the linear response regime. The length scale of mutual diffusion for PolyILs was found to be ~0.60 nm, which is reasonable and in excellent agreement with values reported in (*37*) using a different analysis of the BDS data. We should point out that the value of L_m estimated here is $\sim \sqrt{6}$ times the value reported in our previous work (*31*), which means that the mutual diffusion coefficient D_m is ~6 times the self-diffusion constant of the counterions (estimated using PFG-NMR measurements), in contrast to strict enforcement of D_m being equal to the self-diffusion constant of counterions used in (*31*) for estimating L_m. The fit parameters were plugged into Eq. 1 to construct capacitance of the electrode-PolyIL interfaces, and these results are shown in Fig. 2B. Derivation of Eq. 1 from the electrode polarization model, analyzed in the steady state, is presented in Appendix B in the Supplementary Materials. Briefly, capacitance can be shown to be

$$C_{\text{interface}} = \frac{\epsilon_o \epsilon_r}{L_m \lambda_s} \frac{[\cosh(d/L_m) - 1]}{\left[\frac{\cosh(d/L_m)}{L_m} + \frac{\sinh(d/L_m)}{\lambda_s}\right]} \quad (1)$$

where ϵ_o, ϵ_r, L_m, λ_s, and $2(d + \lambda_s)$ are the permittivity of vacuum, static dielectric constant of the film, length scale of mutual diffusion, apparent thickness of low-dielectric layer on each electrode, and apparent total distance between the electrodes, respectively. Also, $\lambda_s = l_s\epsilon_r/\epsilon_s$, where l_s and ϵ_s are the real thickness and static dielectric constant of the low-dielectric layer, respectively. Except for d, which was set by experimental conditions used to measure BDS spectra, all of the parameters were readily obtained by fitting the BDS spectra. Unfortunately, l_s and ϵ_s are not directly accessible from the BDS spectra. This is because the impedance measured using BDS shows dependence on l_s and ϵ_s only via λ_s. We should point out that in the limit, where $d/L_m \to \infty$, $1/\cosh(d/L_m) \to 0$, and $\tanh(d/L_m) \to 1$, Eq. 1 can be simplified as $C_{\text{interface}} = C^{\infty}_{\text{interface}}$, where

$$C^{\infty}_{\text{interface}} = \left[\frac{L_m}{\epsilon_o \epsilon_r} + \frac{l_s}{\epsilon_o \epsilon_s}\right]^{-1} \quad (2)$$

Equation 2 simply shows that the low-dielectric layer and another layer characterized by L_m and relative permittivity $\epsilon_o\epsilon_r$ act as two capacitors in series leading to sequential voltage drop across each of them. Also, in the limit of $d/L_m \to \infty$, the capacitance is independent of the parameter d.

The camel shape of capacitance-voltage curves shown in Fig. 2B is qualitatively similar to the one predicted in atomistic MD simulations of ILs on rough surfaces (*21*). The two maxima have roughly the same positions. Unexpectedly, we did not detect any substantial asymmetry in the shape of the individual peaks as would be expected based on studies with ILs because of the different sizes of the ions on the chains and their counterions [e.g., van der Waals radii of the mobile counterion (*38*) and the monomer (*39*) used in this study

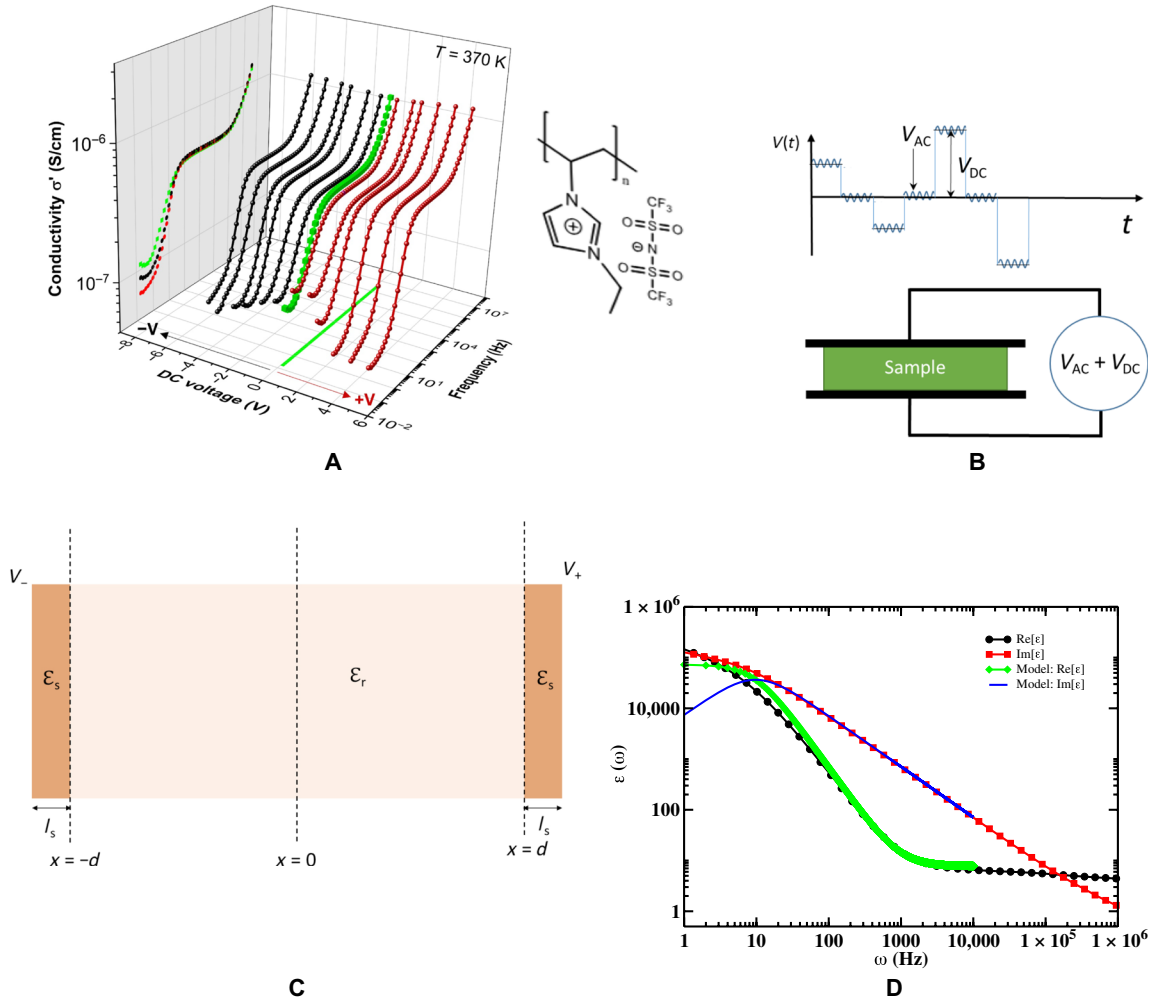

Fig. 1. Details of the BDS measurements, chemical structure of PolyIL studied in this work along with the electrode polarization model used for interpretaion of experimental results. (**A**) BDS spectra plotted versus frequency and applied DC bias, along with the chemical structure of the PolyIL studied in this work. (**B**) Schematics of the applied voltage pulses involving DC and AC components as a function of time (*t*). (**C**) Schematic of the system studied using the Rayleighian approach (*31*) showing a film sandwiched between two planar parallel electrodes. The applied voltage at the right and the left electrode is V_+ and V_-, respectively. The material studied in this work, i.e., PolyIL and its counterions, has a relative permittivity of ϵ_r, and each electrode has an effective interfacial layer of the same thickness, l_s, having a dielectric of $\epsilon_s < \epsilon_r$. (**D**) An example showing fittings of real and imaginary parts of BDS spectra using the electrode polarization model (*31*) based on the Rayleighian approach.

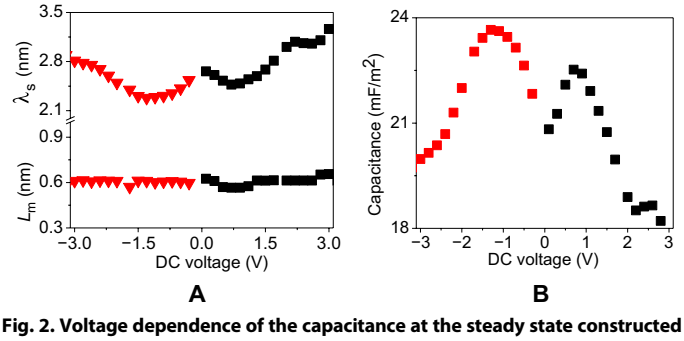

Fig. 2. Voltage dependence of the capacitance at the steady state constructed from the apparent thickness of the low-dielectric layer and the length scale of mutual diffusion. (**A**) Apparent thickness of the low-dielectric layer (λ_s) and the length scale of mutual diffusion (L_m) obtained from the fitting of the BDS data for the PolyIL at 370 K with the Rayleighian-based electrode polarization model. Static dielectric constant of the film (ϵ_r) was also obtained by fitting spectra at zero DC voltage and kept constant as a function of the applied voltage. In particular, $\epsilon_r = 7.7$ and $d = 25\,\mu m$ were used in generating these plots. (**B**) Capacitance calculated from Eq. 1 using parameters shown in (A).

are estimated to be 0.33 and 0.57 nm, respectively]. As the shape of the capacitance-voltage curve is dictated by the low-dielectric layer, such a lack of asymmetry in the curve implies that reorganization of the low-dielectric layer in applied voltages is almost symmetric as shown in Fig. 2A. However, because of the lack of information about molecular mechanisms underlying reorganization of the low-dielectric layer, reasons for the symmetric λ_s-voltage curve (cf. Fig. 2A) are not clear. Note that the apparent thickness of the low-dielectric layer at 0 V is not zero and has a value of ~2.7 nm (cf. Fig. 2A). The observed nonzero initial thicknesses can originate from the physically adsorbed layer of PolyILs and/or can be due to the rough layer of native oxides found on most of the electrodes. This statement is in line with results of reflectivity measurements (cf. Fig. 3B), which revealed the presence of an interfacial layer without any applied bias with a thickness of 1.4 ± 0.3 nm while the scattering length density (SLD) of the interfacial layer is 1.50×10^{-6} Å^{-2}, which is lower than a bulk polymer film value of 2.55×10^{-6} Å^{-2}.

Note that the SLD value for bulk polymer is in good agreement with the theoretical value of 2.63×10^{-6} Å^{-2} calculated based on the pure polymer density. The disparity in the SLD values for bulk and interface can be attributed to a decrease in counterion density in the interfacial region, which lowers its SLD value closer to the value expected of the polymer without a mobile counterion. Unfortunately, direct comparisons between neutron and BDS studies are not possible due to the different types of substrates used in these measurements. Nevertheless, it should be clear that both the silicon and metallic electrode surfaces had preadsorbed layers, whose voltage dependence dictated the capacitance-voltage relations. Transformation of this preadsorbed layer with changes in applied voltage determined the capacitance-voltage relation, highlighting that the quality and chemistry of preadsorbed layer are important in designing efficient energy storage devices. Similar adsorbed layers have been observed in atomistic MD simulations of polymerized ILs on neutral and charged substrates (*40*).

In constructing capacitance-voltage relations from BDS measurements, we have used a minimal model with simplifying assumptions such as symmetry of low-dielectric layers on the two electrodes and ignored explicit nonlinear dependence of the surface charge on applied voltage and asymmetry in molar volume of monomers with respect to counterions. To go beyond these simplifying assumptions and study their effects on capacitance-voltage curves, we have numerically solved (*41*, *42*) underlying eqs. A-1 to A-4 of the electrode polarization model in a steady state. Representative results obtained from the numerical solutions are shown in Fig. 4. In the absence of any molecular model, voltage dependence of the λ_s was ignored while solving the equations. For experimentally studied systems for which $L_m/d \to 0$, the right panel in Fig. 4 shows that capacitance in a steady state is mainly dictated by the low-dielectric layer, which yields nonzero capacitance at zero applied voltage. However, if $L_m/d \gg 1$, then there is an additional contribution to the capacitance, which is voltage dependent and decreases with an increase in the applied voltage, V. It can be readily shown that the capacitance must decrease as $V^{-1/2}$ in the absence of the low-dielectric layer (see Appendix C for details), and this is a direct consequence of the crowding enforced by the local incompressibility condition in the model. Specifically, taking $\lambda_s = 0$ for an applied voltage V, capacitance can be derived to be

$$C = \frac{\sqrt{8\pi l_B \rho_{co}}\left| z_p \nu_r - \frac{\exp(-(z_c - z_p \nu_r)\overline{V})}{1 + \frac{\nu_r}{N_p}\bar{\phi}_c \exp(-(z_c - z_p \nu_r)\overline{V})}\right|}{2\sqrt{\left|-z_p \nu_r \overline{V} + \frac{N_p}{\nu_r \bar{\phi}_c}\ln\left(\frac{1 + \frac{\nu_r}{N_p}\bar{\phi}_c \exp(-(z_c - z_p \nu_r)\overline{V})}{1 + \frac{\nu_r}{N_p}\bar{\phi}_c}\right)\right|}} \quad (3)$$

where $\overline{V} = eV/k_B T$ is the dimensionless voltage so that e is the charge of an electron; k_B is the Boltzmann constant; T is the temperature; l_B is the Bjerrum length; z_c and $1/\rho_{co}$ are the valency and the molar volume of the counterions, respectively; ν_r is the ratio of molar volume of the counterions to the monomers; z_p is the valency of a monomer; and N_p is the number of Kuhn segments along a polymer chain. The only unknown in this equation is $\bar{\phi}_c$, which is an integration constant. Equation 3 shows that the capacitance-voltage relations are weakly dependent on N_p, which is confirmed by numerical solutions in Appendix D. Comparing Figs. 2B and 4, we conclude that if the dependence of λ_s on applied voltage was to be ignored, then the capacitance should either be independent or decrease with an increase in applied voltage similar to the curves shown in Fig. 4. Nevertheless, letting λ_s vary with applied voltage led to the camel-shaped capacitance-voltage curve, indicating the strong dependence of the capacitance on the low-dielectric layer. Note that our treatment of the low-dielectric layer is conceptually similar to the Stern layer in a classical treatment of electric double layers in dilute solutions, as presented by Grahame in 1954 (*2*). In addition, temperature can be varied to alter magnitude of the steady-state capacitance at 0 V due to changes in apparent thickness of the low-dielectric layer (*31*). However, qualitative features of capacitance-voltage relations are expected to be similar to Fig. 2.

CONCLUSIONS

We have studied electrode-PolyIL interfaces using BDS, neutron reflectometry, and modeling based on the Rayleighian approach. It was shown that a preadsorbed layer exists at the electrode at zero applied voltage, which dictates measured impedance and capacitance of the electrode-PolyIL interfaces. The preadsorbed layer, which was treated as a low-dielectric layer in the electrode polarization model studied here, is expected to be present in most of the other films

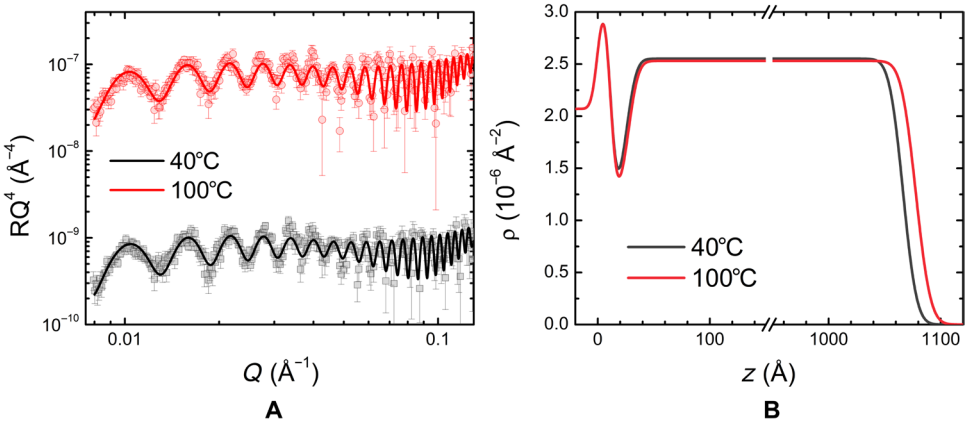

Fig. 3. Results from neutron reflectometry showing the presence of an interfacial layer in films prepared by depositing the PolyIL at Si/SiO$_2$ substrate. Neutron reflectivity (*R*) (**A**) and the associated SLD (ρ) models (**B**) of the PolyIL films. Black squares and red circles indicate measurements at 40° and 100°C, respectively. The solid lines in the reflectivity plots represent the best fits generated by the SLD profiles shown in (B). These profiles correspond to the PolyIL deposited on the Si/SiO$_2$ substrate.

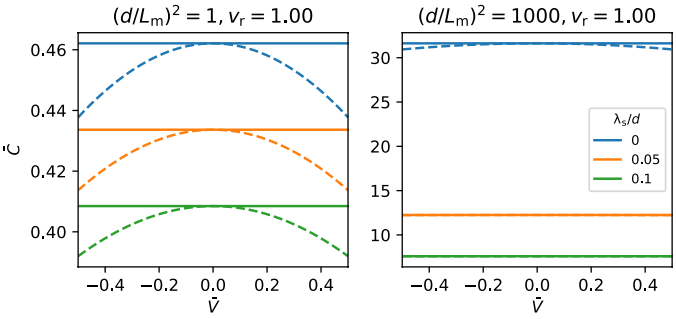

Fig. 4. Results obtained for capacitance-voltage relations by numerically solving the underlying equations of the electrode polarization model in a steady state (see Appendix D in the Supporting Materials for the details). Here, v_r is the ratio of molar volume of a counterion to that of a monomer, $\bar{C}$ is the capacitance (in units of $\epsilon_o\epsilon_r/d$) and $\bar{V} = eV/k_BT$, V being the applied voltage. Solid lines are obtained by solving an approximate set of equations enforcing weak inhomogeneity, and dashed lines represent numerical solutions beyond the limit of weak inhomogeneity. More details can be found in the Supplementary Materials.

containing similarly charged PolyILs. Such an expectation results from the hypothesis that adsorption of the PolyILs is driven by their attraction toward negatively charged surfaces and metallic electrodes. Not only did we estimate the apparent thickness of the low-dielectric layer from the BDS spectrum, but we also found the thickness to exhibit a nonmonotonic dependence on the applied voltages. The nonmonotonic dependence manifests in a similar dependence of the capacitance-voltage curves for the films. We found that the preadsorbed layer at 0 V plays an important role in determining changes in the interfacial layer thickness in an applied voltage up to 1 V, as we see clear monotonic decrease in its thickness with applied electric field. These changes can be associated with rearrangement of the already adsorbed layer similar to those observed in atomistic simulations (*40*). Capacitance-voltage curves are found to be camel-shaped exhibiting almost no substantial asymmetry with the reversal of voltage. Our numerical investigations revealed that size asymmetry between monomers and counterions does not affect the capacitance-voltage relations significantly. This suggests that only the preadsorbed layer near the electrode contributes substantially to the capacitance. Last, the capacitance is, on average, found to be ~22 mF/cm^2 for the PolyIL studied in this work, and the shape of capacitance-voltage curve is qualitatively similar to the corresponding IL. As an outlook, preadsorbed layers are expected to be present in most of the films containing similarly charged polymers, and this study should be of interest to researchers engaged in research related to energy storage and harvesting devices.

MATERIALS AND METHODS

BDS measurements

The chemical structure of the PolyIL used in this study is presented in Fig. 1A. Synthesis of poly(*N*-vinyl ethyl imidazolium) is detailed elsewhere (*31*, *43*). Direct measurements of the molecular weight of the PolyIL are challenging and were not performed here as it required a combination of certain solvents to neutralize the charge of the polymer, which are not known. However, some information about molecular weight and dispersity of the PolyIL is known. Specifically, the PolyIL was synthesized from poly(*N*-vinyl imidazole). The latter was synthesized using conditions reported in (*44*), and the reaction conditions would give M_n = 42,000 g/mol with a dispersity of 1.84. The BDS measurements were performed in a frequency range 10^{-2} to 10^7 Hz using an Alpha-A analyzer from Novocontrol. DC voltages of different polarities and amplitudes were applied to the sample. For BDS measurements, the sample of PolyILs was spin-coated from an acetone solution between two stainless steel plates separated by silica fibers with a thickness of 50 μm. The spectra were accumulated at 97°C, which is 30°C above the glass transition temperature (T_g) of this polymer. Before the measurements, the temperature was stabilized within 0.2 K by a Quattro temperature controller, also provided by Novocontrol. In the experiments with DC voltage, the AC amplitude was kept at 0.01 V, while DC bias was changed gradually from 0.1 to 20 V. Spectra obtained after application of different DC voltages are presented in Fig. 1A. In the experiments with DC voltage, first positive bias was applied, followed by zero bias and negative bias at each frequency. A schematic of the experimental protocol is presented in Fig. 1B. Note that spectra were analyzed in the range of −3 to 3 V in the absence of Faradaic current, where changes in the spectra were reversible.

Rayleighian approach–based model for electrode polarization and capacitance

Fitting BDS spectra using the model

We used the Rayleighian approach (*29*–*31*) for understanding capacitance-voltage relations in films of PolyILs. Recently, we have used the approach to develop a model for electrode polarization phenomenon (*31*), which can be studied using BDS measurements. A brief description of the model is presented in Appendix A in the Supplementary Materials. In this work, the same model for electrode polarization was used to fit the BDS spectra, and the fit parameters were used to construct capacitance of the films using an analytical expression derived in the current work. An example showing typical fits of the BDS spectra is presented in Fig. 1D. Briefly, fittings of the BDS spectra were performed only for the peak region in the ratio of imaginary and real parts of the frequency-dependent dielectric response [known as tan δ or the loss tangent in the literature on the BDS (*45*)]. The main advantage of fitting the peak is that the fit results are independent of the values of the static permittivity of the medium, leading to a reduction in the number of fit parameters. Also, the location of the peak provides an estimate of the characteristic time involved in the electrode polarization, which provides reasonable initial estimates of the fit parameters. Specifically, the fitting was performed through constrained multivariable optimization of the ratio of the imaginary and the real part of eq. A-5 in the Supplementary Materials to the corresponding BDS data using the software package Mathematica. Three parameters were optimized: the characteristic time scale of the mutual diffusion (τ_m), the apparent thickness of a low-dielectric layer with respect to the separation between the electrodes (λ_s/d), and the length scale of mutual diffusion (L_m). The apparent thickness of the low-dielectric layer (λ_s) was assumed to be the same on each electrode, which were taken to be separated by distance 2d so that the total distance between the electrodes was taken to be $2(d + \lambda_s)$ (see Fig. 1C for a schematic). Numerical results obtained by solving equations (eqs. A-1 to A-4) for the electrode polarization model showed that asymmetry in sizes of the low-dielectric layers on two sides of the films had negligible effect on capacitance-voltage relations. For the fitting of the

data, d was taken to be 25 μm. Lower limits of the three parameters were constrained to zero, and the upper limits were chosen as follows. The upper limit of λ_s was set to an arbitrarily high value of 100 nm as it did not have any significant impact on the fitting. However, the choice of the upper limit of τ_m had a significant impact on the fit results. If the choice was too far off from the correct value ($\sim 1/\omega_{peak}$, where ω_{peak} is the circular frequency for the peak in tan δ), then we could not fit the experimental results. Thus, the upper limit of τ_m was chosen close to $\sim 1/\omega_{peak}$. The upper limit of L_m was chosen on the basis of the complimentary PFG-NMR measurements of the diffusion constants presented in our previous work (*31*). In particular, we used the relation $D_m = L_m^2/\tau_m$ to estimate the mutual diffusion constant (D_m). For different choices of the upper limit of L_m, the peak in tan δ can be fitted using eq. A-5, but the extracted D_m may be orders of magnitude off from the PFG-NMR results. This results from the fact that there are multiple parameter sets, which can fit the same experimental data [see (*31*) for the details]. For the results presented in Fig. 2A, the upper limit of L_m was set at 1.5 nm for all the PolyIL samples. The static permittivity of the medium ($\epsilon_0\epsilon_r$) was determined by fitting the real and the imaginary parts of the dielectric response at the lowest voltage. In particular, fitting with one additional multiplicative factor was performed for ϵ' and ϵ'' by using eq. A-5 with the extracted τ_m, λ_s/d, and L_m. However, we kept $\epsilon_0\epsilon_r$ fixed as a function of DC voltage as we did not expect any dielectric saturation effect for small applied voltages. After estimating the four parameters from the BDS spectra, capacitance at the steady state was determined by using Eq. 1 (see Appendix B in the Supplementary Materials for its derivation). However, Eq. 1 has no explicit dependence on the applied DC voltage. To understand the capacitance-voltage relations, we assumed that voltage dependence appears implicitly via the thickness of the low-dielectric layer (λ_s) and the length scale of mutual diffusion (L_m). Thus, we let them vary while fitting the experimental BDS data at different voltages. In other words, we determined voltage dependencies of λ_s and L_m from the BDS data.

Numerical results obtained from the model

To understand explicit dependence of the capacitance on applied voltage, we solved the equations appearing in the electrode polarization model and studied the effects of various parameters on capacitance-voltage curves (see Appendices C and D in the Supplementary Materials). Key representative results are presented in Fig. 4 and figs. S2 to S4, and details about numerical methods are presented in the Supplementary Materials.

Neutron reflectometry

To probe structure in the thin films, we performed neutron reflectometry measurements (*32*–*35*). The PolyIL film was spin-coated on a silicon wafer and placed in a heating cell for the measurements. The measurements were performed at 40° and 100°C. Apart from the oscillations originating from the film interference, the reflectivity decayed with the expected Q^4 (Q being the wave vector) dependence up to $\sim$ 0.13 $Å^{-1}$. For higher values of Q, the reflected intensity became indistinguishable from the substrate background scattering (i.e., reflectivity, $R < 10^{-6}$); data beyond this Q range were not included in the fitting. Models to the reflectivity data were simulated by generating SLD profiles. Each layer was associated with individual thickness, SLD (ρ), and interfacial width (σ). The theoretical SLDs, estimated using the compositions and densities of the polymer with counterion (2.63×10^{-6} $Å^{-2}$), polymer without counterion (1.18×10^{-6} $Å^{-2}$), and the counterion alone (2.76×10^{-6} $Å^{-2}$), were used as initial fitting parameters and limits of the fitting. The fitting was performed using three layers, which consisted of (i) the native oxide layer, (ii) an interface between the silicon wafer and the polymer, and (iii) the bulk polymer film. We also fitted the reflectivity curves including an additional air-polymer interface layer. However, the resulting fits were similar to the ones without the added layer, suggesting that the three-layer model was adequate for describing this interface. The latter statement is also supported by literature data obtained for air–ionic liquid interfaces (*15*). Furthermore, in our case, fitting with only a single polymer layer without the depleted zone proved to be inadequate. Between both fits, values of ρ for the silicon (Si), oxide layer (SiO_2), and air in addition to σ for the substrate/(1) and (1)/(2) and (2)/(3) interfaces were held constant, since these values were found to not depend significantly on the temperature. The thickness of the native oxide was fixed to be 1.1 nm. The thickness of the bulk polymer was found to be 104 to 105 nm, in agreement with our ellipsometry measurements. The SLD and thickness of the interfacial layer were found to be highly coupled. To eliminate this codependence, the SLD was restricted to the lower limit of the pure polymer (without counterions), while the thickness was free to vary. For the bulk polymer layer, both thickness and ρ were free to assume any values. The spectra for 0 V overlaid for 40° and 100°C together with the fittings are presented in Fig. 3A. The SLD profiles generated from the fittings are presented in Fig. 3B.

SUPPLEMENTARY MATERIALS

Supplementary material for this article is available at http://advances.sciencemag.org/cgi/content/full/6/26/eaba7952/DC1

REFERENCES AND NOTES

1. D. C. Grahame, The electrical double layer and the theory of electrocapillarity. *Chem. Rev.* **41**, 441–501 (1947).
2. D. C. Grahame, Differential capacity of mercury in aqueous sodium fluoride solutions. I. Effect of concentration at 25. *J. Am. Chem. Soc.* **76**, 4819–4823 (1954).
3. E. Verwey, J. Overbeek, K. van Nes, *Theory of the Stability of Lyophobic Colloids: The Interaction of Sol Particles Having an Electric Double Layer* (Elsevier Publishing Company, 1948).
4. S. L. Carnie, G. M. Torrie, in *The Statistical Mechanics of the Electrical Double Layer* (John Wiley & Sons Ltd., 2007), pp. 141–253.
5. J. Israelachvili, *Intermolecular and Surface Forces, Intermolecular and Surface Forces* (Elsevier Science, 2015).
6. A. A. Kornyshev, Double-layer in ionic liquids: Paradigm change? *J. Phys. Chem. B* **111**, 5545–5557 (2007).
7. M. V. Fedorov, A. A. Kornyshev, Ionic liquids at electrified interfaces. *Chem. Rev.* **114**, 2978–3036 (2014).
8. A. González, E. Goikolea, J. A. Barrena, R. Mysyk, Review on supercapacitors: Technologies and materials. *Renew. Sustain. Energy Rev.* **58**, 1189–1206 (2016).
9. V. Lockett, R. Sedev, S. Harmer, J. Ralston, M. Horne, T. Rodopoulos, Orientation and mutual location of ions at the surface of ionic liquids. *Phys. Chem. Chem. Phys.* **12**, 13816–13827 (2010).
10. V. Lockett, M. Horne, R. Sedev, T. Rodopoulos, J. Ralston, Differential capacitance of the double layer at the electrode/ionic liquids interface. *Phys. Chem. Chem. Phys.* **12**, 12499–12512 (2010).
11. M. Z. Bazant, B. D. Storey, A. A. Kornyshev, Double layer in ionic liquids: Overscreening versus crowding. *Phys. Rev. Lett.* **106**, 046102 (2011).
12. S. Perkin, Ionic liquids in confined geometries. *Phys. Chem. Chem. Phys.* **14**, 5052–5062 (2012).
13. Y. Nakayama, D. Andelman, Differential capacitance of the electric double layer: The interplay between ion finite size and dielectric decrement. *J. Chem. Phys.* **142**, 044706 (2015).
14. A. M. Smith, A. A. Lee, S. Perkin, The electrostatic screening length in concentrated electrolytes increases with concentration. *J. Phys. Chem. Lett.* **7**, 2157–2163 (2016).

15. M. Mezger, H. Schröder, H. Reichert, S. Schramm, J. S. Okasinski, S. Schöder, V. Honkimäki, M. Deutsch, B. M. Ocko, J. Ralston, M. Rohwerder, M. Stratmann, H. Dosch, Molecular layering of fluorinated ionic liquids at a charged sapphire (0001) surface. *Science* **322**, 424–428 (2008).
16. M. A. Gebbie, H. A. Dobbs, M. Valtiner, J. N. Israelachvili, Long-range electrostatic screening in ionic liquids. *Proc. Natl. Acad. Sci. U.S.A.* **112**, 7432–7437 (2015).
17. M. Drüschler, N. Borisenko, J. Wallauer, C. Winter, B. Huber, F. Endres, B. Roling, New insights into the interface between a single-crystalline metal electrode and an extremely pure ionic liquid: Slow interfacial processes and the influence of temperature on interfacial dynamics. *Phys. Chem. Chem. Phys.* **14**, 5090–5099 (2012).
18. H. K. Kashyap, C. S. Santos, H. V. R. Annapureddy, N. S. Murthy, C. J. Margulis, E. W. Castner Jr, Temperature-dependent structure of ionic liquids: X-ray scattering and simulations. *Faraday Discuss.* **154**, 133–143 (2012).
19. B. Roling, M. Drüschler, B. Huber, Slow and fast capacitive process taking place at the ionic liquid/electrode interface. *Faraday Discuss.* **154**, 303–311 (2012).
20. S. Tazi, M. Salanne, C. Simon, P. Turq, M. Pounds, P. A. Madden, Potential-induced ordering transition of the adsorbed layer at the ionic liquid/electrified metal interface. *J. Phys. Chem. B* **114**, 8453–8459 (2010).
21. J. Vatamanu, O. Borodin, G. D. Smith, Molecular simulations of the electric double layer structure, differential capacitance, and charging kinetics for *N*-methyl-*N*-propylpyrrolidinium bis(fluorosulfonyl)imide at graphite electrodes. *J. Phys. Chem. B* **115**, 3073–3084 (2011).
22. L. Xing, J. Vatamanu, G. D. Smith, D. Bedrov, Nanopatterning of Electrode surfaces as a potential route to improve the energy density of electric double-layer capacitors: Insight from molecular simulations. *J. Phys. Chem.* **3**, 1124–1129 (2012).
23. G. Feng, P. T. Cummings, Supercapacitor capacitance exhibits oscillatory behavior as a function of nanopore size. *J. Phys. Chem. Lett.* **2**, 2859–2864 (2011).
24. D.-e. Jiang, Z. Jin, J. Wu, Oscillation of capacitance inside nanopores. *Nano Lett.* **11**, 5373–5377 (2011).
25. C. Merlet, C. Péan, B. Rotenberg, P. A. Madden, P. Simon, M. Salanne, Simulating supercapacitors: Can we model electrodes as constant charge surfaces? *J. Phys. Chem. Lett.* **4**, 264–268 (2013).
26. S. Lamperski, C. W. Outhwaite, L. B. Bhuiyan, The electric double-layer differential capacitance at and near zero surface charge for a restricted primitive model electrolyte. *J. Phys. Chem. B* **113**, 8925–8929 (2009).
27. M. B. Armand, P. G. Bruce, M. Forsyth, B. Scrosati, W. Wieczorek, in *Polymer Electrolytes* (John Wiley & Sons Ltd., 2011), chap. 1, pp. 1–31.
28. M. Armand, F. Endres, D. R. MacFarlane, H. Ohno, B. Scrosati, Ionic-liquid materials for the electrochemical challenges of the future. *Nat. Mater.* **8**, 621–629 (2009).
29. L. Onsager, Theories and problems of liquid diffusion. *Ann. N. Y. Acad. Sci.* **46**, 241–265 (1945).
30. M. Doi, Onsager's variational principle in soft matter. *J. Phys. Condens. Matter* **23**, 284118 (2011).
31. R. Kumar, J. P. Mahalik, V. Bocharova, E. W. Stacy, C. Gainaru, T. Saito, M. P. Gobet, S. Greenbaum, B. G. Sumpter, A. P. Sokolov, A Rayleighian approach for modeling kinetics of ionic transport in polymeric media. *J. Chem. Phys.* **146**, 064902 (2017).
32. R. Kumar, B. S. Lokitz, S. W. Sides, J. Chen, W. T. Heller, J. F. Ankner, J. F. Browning, S. M. Kilbey II, B. G. Sumpter, Microphase separation in thin films of lamellar forming polydisperse di-block copolymers. *RSC Adv.* **5**, 21336–21348 (2015).
33. J. P. Mahalik, Y. Yang, C. Deodhar, J. F. Ankner, B. S. Lokitz, S. M. Kilbey II, B. G. Sumpter, R. Kumar, Monomer volume fraction profiles in pH responsive planar polyelectrolyte brushes. *J. Polym. Sci. B* **54**, 956–964 (2016).
34. J. P. Mahalik, J. W. Dugger, S. W. Sides, B. G. Sumpter, V. Lauter, R. Kumar, Interpreting neutron reflectivity profiles of diblock copolymer nanocomposite thin films using hybrid particle-field simulations. *Macromolecules* **51**, 3116–3125 (2018).
35. J. W. Dugger, W. Li, M. Chen, T. E. Long, R. J. L. Welbourn, M. W. A. Skoda, J. F. Browning, R. Kumar, B. S. Lokitz, Nanoscale resolution of electric-field induced motion in ionic diblock copolymer thin films. *ACS Appl. Mater. Interfaces* **10**, 32678–32687 (2018).
36. J.-H. Choi, W. Xie, Y. Gu, C. D. Frisbie, T. P. Lodge, Single ion conducting, polymerized ionic liquid triblock copolymer films: High capacitance electrolyte gates for n-type transistors. *ACS Appl. Mater. Interfaces* **7**, 7294–7302 (2015).
37. C. Gainaru, E. W. Stacy, V. Bocharova, M. Gobet, A. P. Holt, T. Saito, S. Greenbaum, A. P. Sokolov, Mechanism of conductivity relaxation in liquid and polymeric electrolytes: Direct link between conductivity and diffusivity. *J. Phys. Chem. B* **120**, 11074–11083 (2016).
38. M. Ue, A. Murakami, S. Nakamura, A convenient method to estimate ion size for electrolyte materials design. *J. Electrochem. Soc.* **149**, A1385 (2002).
39. B. Doughty, A.-C. Genix, I. Popov, B. Li, S. Zhao, T. Saito, D. A. Lutterman, R. L. Sacci, B. G. Sumpter, Z. Wojnarowska, V. Bocharova, Structural correlations tailor conductive properties in polymerized ionic liquids. *Phys. Chem. Chem. Phys.* **21**, 14775–14785 (2019).
40. Z. Yu, C. Fang, J. Huang, B. G. Sumpter, R. Qiao, Molecular structure and dynamics of interfacial polymerized ionic liquids. *J. Phys. Chem. C* **122**, 22494–22503 (2018).
41. T. A. Driscoll, N. Hale, L. N. Trefethen, *Chebfun Guide* (Pafnuty Publications, 2014).
42. A. Birkisson, T. A. Driscoll, Automatic Fréchet Differentiation for the numerical solution of boundary-value problems. *ACM Trans. Math. Software* **38**, 1–29 (2012).
43. Z. Wojnarowska, H. Feng, Y. Fu, S. Cheng, B. Carroll, R. Kumar, V. N. Novikov, A. M. Kisliuk, T. Saito, N.-G. Kang, J. W. Mays, A. P. Sokolov, V. Bocharova, Effect of chain rigidity on the decoupling of ion motion from segmental relaxation in polymerized ionic liquids: Ambient and elevated pressure studies. *Macromolecules* **50**, 6710–6721 (2017).
44. M. D. Green, D. Salas-de la Cruz, Y. Ye, J. M. Layman, Y. A. Elabd, K. I. Winey, T. E. Long, Alkyl-substituted *N*-vinylimidazolium polymerized ionic liquids: Thermal properties and ionic conductivities. *Macromol. Chem. Phys.* **212**, 2522–2528 (2011).
45. F. Kremer, *Broadband Dielectric Spectroscopy* (Springer-Verlag, 2003).

Acknowledgments: We gratefully acknowledge contributions from G. Smith related to neutron reflectivity experiments in the early stages of the works presented in this manuscript. **Funding:** This research was sponsored by the Laboratory Directed Research and Development (LDRD) Program of Oak Ridge National Laboratory (ORNL), managed by UT-Battelle, LLC, for the U.S. Department of Energy. The research was conducted at the Center for Nanophase Materials Sciences, which is a U.S. Department of Energy Office of Science User Facility. K.S.S. was supported by the Department of Energy Computational Science Graduate Fellowship program under grant no. DE-FG02-97ER25308. A.P.S. and B.G.S. acknowledge support from the Division of Materials Sciences and Engineering, DOE Office of Basic Energy Sciences. **Author contributions:** R.K., J.P.M., K.S.S., and B.G.S. contributed to the computational aspects in this work. Z.W., V.B., and A.P.S. contributed to the materials and BDS measurements. A.E. and J.F.A. contributed to the neutron reflectivity–based analysis presented in the manuscript. **Competing interests:** The authors declare that they have no competing interests. **Data and materials availability:** All data needed to evaluate the conclusions in the paper are present in the paper and/or the Supplementary Materials. Additional data related to this paper may be requested from the authors.

Submitted 6 January 2020
Accepted 15 May 2020
Published 26 June 2020
10.1126/sciadv.aba7952

Citation: R. Kumar, J. P. Mahalik, K. S. Silmore, Z. Wojnarowska, A. Erwin, J. F. Ankner, A. P. Sokolov, B. G. Sumpter, V. Bocharova, Capacitance of thin films containing polymerized ionic liquids. *Sci. Adv.* **6**, eaba7952 (2020).

Science Advances

Capacitance of thin films containing polymerized ionic liquids

Rajeev Kumar, Jyoti P. Mahalik, Kevin S. Silmore, Zaneta Wojnarowska, Andrew Erwin, John F. Ankner, Alexei P. Sokolov, Bobby G. Sumpter and Vera Bocharova

Sci Adv **6** (26), eaba7952.
DOI: 10.1126/sciadv.aba7952

Science Advances (ISSN 2375-2548) is published by the American Association for the Advancement of Science, 1200 New York Avenue NW, Washington, DC 20005. The title *Science Advances* is a registered trademark of AAAS.